Available online at www.sciencedirect.com

ScienceDirect

Nuclear Physics B 967 (2021) 115404

NUCLEAR PHYSICS B

www.elsevier.com/locate/nuclphysb

Characterisation of dark matter in direct detection experiments: Singlino versus Higgsino

Yaşar Hiçyılmaz [a,b,*], Stefano Moretti [a]

[a] *School of Physics and Astronomy, University of Southampton, Highfield, Southampton SO17 1BJ, United Kingdom*
[b] *Department of Physics, Balıkesir University, TR10145, Balıkesir, Turkey*

Received 17 January 2021; received in revised form 9 March 2021; accepted 12 April 2021
Available online 16 April 2021
Editor: Hong-Jian He

Abstract

We show how the material used in direct detection experiments of Dark Matter (DM), in the presence of a signal of it, can afford one with the possibility of extracting the nature of the underlying candidate. We do so for the case of a $U(1)'$ Supersymmetric Standard Model (USSM) of E_6 origin, by exploiting benchmark points over its parameter space that yield either a Singlino- or Higgsino-like neutralino as DM candidate, the latter being defined in presence of up-to-date constraints, from low to high energy and from collider to non-collider experiments. However, as our method is general, we also introduce a model-independent description of our analysis, for the purpose of aiding similar studies in other Beyond the Standard Model (BSM) scenarios. This has been made possible by adapting a rather simple χ^2 analysis normally used for signal extraction in direct detection experiments and the procedure has been applied to Xenon, Germanium and Silicon detectors, those showing maximal and complementary sensitivity to gauge- and Higgs-portal induced interactions of DM with their nuclei.

1. Introduction

Understanding the nature of Dark Matter (DM) is one of the most fundamental problems of particle physics and astronomy. Today, the vast majority of particle physicists and astronomers

* Corresponding author.
E-mail addresses: Y.Hicyilmaz@soton.ac.uk (Y. Hiçyılmaz), S.Moretti@soton.ac.uk (S. Moretti).

https://doi.org/10.1016/j.nuclphysb.2021.115404

believe that more than 20 percent of the mass that exists in our universe is composed of non-luminous matter, indeed, called DM. Since 1933, when the astronomer Fritz Zwicky first observed the dispersion of the velocities of the galaxies in the Coma cluster [1], which could only be accounted for by such a new form of matter, no direct information is available about DM (e.g., its mass, spin, composition, the symmetry responsible for its stable structure, how it interacts with the Standard Model (SM) particles, etc.). Further, the existence of DM is one of the most obvious reason to seek Beyond SM (BSM) physics, simply because the SM has no DM candidate. Today, observations on the cosmological scale allow us to quantify the abundance of DM in the universe. Due to the observed abundance, the majority of DM cannot be in baryonic form, since the Big Bang Nucleosynthesis (BBN) puts an upper bound on the density of baryons in the universe [2]. In that case, some BSM scenarios, like Supersymmetry, can provide non-baryonic DM candidates, so-called Weakly Interacting Massive Particles (WIMPs), which are stable, massive and weakly interacting with the ordinary matter. WIMPs are particularly attractive as they can give the right amount of relic abundance in the universe measured by Planck [3] and WMAP [4]. Moreover, WIMPs are experimentally appealing DM candidates because of the possibility of their detection.

Currently, experimental searches for WIMPs as DM are performed under three main approaches. The first of these is searches carried out at colliders, like the Large Hadron Collider (LHC) at CERN. The others are cosmological searches in which the effects of DM are observed directly or indirectly on or under the Earth's surface as well as in space. Searches for DM at colliders assume DM production which relies upon the existence of interactions between the (B)SM particles and the DM particles. Such DM particles pass invisibly through the detector so that the main search channels are events with missing energy, stemming from a collision in which a part of the energy goes to undetected particles, which could indeed be WIMPs.

Indirect detection of DM is based on the idea that WIMPs may self-annihilate into SM particles as a flux of cosmic rays, γ-rays, neutrinos and/or antimatter which can appear as an excess over the expected astrophysical background. Such an excess is expected to be detected at cosmic rays detectors [5], γ-ray telescopes [6] or neutrino observatories [7].

Direct detection of DM, on which we focus in this work, aims at detecting WIMPs via the nuclear recoils that arise from an elastic scattering of a WIMP on a target nucleus. Such scatterings occur in the framework of weak interactions, mostly with the exchange of a Z boson, the so-called Spin-Dependent (SD) scattering for Majorana fermions such as neutralino, and the exchange of a Higgs boson, the so-called Spin-Independent (SI) scattering, between the WIMP and the nuclei of the target material.[1] So, the rate of the interactions is extremely small and it is needed to have low-background detectors, which are generally placed underground to shield from the cosmic ray background. There are many direct detection experiments worldwide, in which different type of nuclear targets are used with various background subtraction techniques [8–20].

From a phenomenological perspective, it is important to determine the type of WIMP DM which satisfies the possible signal observed in any direct detection experiment. A brief review of the ideas and methods to unveil WIMP properties in direct detection experiments can be found in Refs. [21–24]. In order to compare potential WIMP candidates in the same or different theoretical models, we need to know whether different direct detection signals of the DM candidates are

[1] In Supersymmetry (SUSY), sfermion exchanges can contribute to the WIMP-nucleus scattering. However, their contributions are typically small, even for light squarks.

separable. The present work is devoted to the analysis of direct detection signals which belong to two different type of neutralino DM candidates emerging in the same SUSY model, the latter being of E_6 origin with a low energy appearance typical of a $U(1)'$ Supersymmetric Standard Model (UMSSM). In our analysis, we employ a χ^2 test as simple statistical approach to measure the difference between two signals. We use Singlino- and Higgsino-like neutralino solutions, which satisfy all current experimental bounds, as studied in detail in our previous work [25]. This present analysis aims at explaining to what extent such two kind of neutralinos are separable for different exposures and target materials in future direct detection experiments. We also observe the effects of the SI and SD cross sections, local DM density and nuclear form factors on the discrimination of DM direct detection signals using model-independent benchmarks.

The organisation of the paper is the following. We will focus on DM direct detection in Section 2. Then, we present our results in Section 3. Finally, we summarise and conclude in Section 4.

2. Direct detection of dark matter

As mentioned, the idea of DM direct detection relies on the observation of the nuclear recoil caused by the weak interactions of WIMPs with the nuclei in detector materials [26]. The recoil energy of a nucleus after a collision with a DM particle can be written as:

$$E_R = \frac{\mu_N^2 v^2 (1 - \cos\theta_{\rm CM})}{m_N}\,, \tag{1}$$

where $\mu_N = \frac{m_\chi m_N}{m_\chi + m_N}$ is the so-called WIMP-nucleus reduced mass, with m_χ and m_N the masses of the WIMP and nucleus, respectively. Here, v is the relative velocity between the WIMP and nucleus while $\theta_{\rm CM}$ is the scattering angle in the Center-of-Mass (CM) frame. Eq. (1) shows that the amount of transferred energy E_R to the nucleus by the WIMP depends on the scattering angle in the CM frame as well as the two masses and relative velocity. This energy is maximal in the case the WIMP backscatters, i.e., $\theta_{\rm CM} = \pi$, while there is no transferred energy if the WIMP passes through the detector without interaction, i.e., $\theta_{\rm CM} = 0$. So, the maximal recoil energy of a nucleus scattered by a WIMP for a given velocity v is obtained as:

$$E_{\rm max}(v) = \frac{2\mu_N^2 v^2}{m_N}\,. \tag{2}$$

Moreover the minimal velocity $v_{\rm min}$ for a WIMP mass m_χ to be able to induce a nuclear recoil of energy E_R is

$$v_{\rm min}(E_R) = \sqrt{\frac{E_R m_N}{2\mu_N^2}}\,. \tag{3}$$

In Eq. (1), if we express the recoil energy E_R as a function of the mass of the target nucleus m_N for any given DM mass m_χ, with velocity v and $\theta_{\rm CM} = \pi$, it can be seen that E_R is maximal in the case of $m_N = m_\chi$, which satisfies the equation $dE_R/dm_N = 0$. This means that the maximal transfer of energy, i.e., the maximal recoil energy, for a given WIMP mass takes place when using a target nucleus with mass approximately equal to that of the WIMP. As a consequence, the sensitivity of a detector increases as the mass of the nucleus to be used as a target in the detector get closer to the mass of the WIMP to be probed in the detector. Heavier nuclei will give

a detector more sensitive to heavier WIMPs. In fact, other than for discovery, the detector sensitivity is also important for the differentiation of possible signals, so a dedicated detector (i.e., with suitable material chosen) could be designed in responsive mode to a discovery in another medium.

The differential event rate, called the nuclear recoil spectrum or the nuclear recoil energy distribution, expressed in terms of the number of events per unit energy per unit time per unit target material mass (in general /keV/kg/day, referred to as a differential rate unit) for a WIMP with mass m_χ and a nucleus with mass m_N is given by [27]

$$\frac{dN}{dE_R} = \frac{\rho_0}{m_N m_\chi} \int\limits_{v>v_{\min}} v f(v) \frac{d\sigma}{dE_R}(v, E_R)\, dv\,, \tag{4}$$

where ρ_0 is the local WIMP density, $\frac{d\sigma}{dE_R}(v, E_R)$ is the differential cross section for the WIMP-nucleus elastic scattering and $f(v)$ is the WIMP speed distribution in the detector frame. In this work, we take into account two different speed distribution models, which are the standard isotropic Maxwellian one and its updated version, so-called SHM++ [28], in order to investigate the effects of astrophysical uncertainties on the local DM density. The lower limit of the integration over WIMP speed $v_{\min}$ is equal to the minimal WIMP velocity shown in Eq. (3) while the upper limit is the maximum speed in the Galactic rest frame for WIMPs which are gravitationally bound to the Milky Way. The total number of recoil events (per kilogram per day) can be found by integrating the differential event rate over all the possible recoil energies:

$$N = \int\limits_{E_T}^{E\max} dE_R \frac{\rho_0}{m_N m_\chi} \int\limits_{v>v_{\min}} v f(v) \frac{d\sigma}{dE_R}(v, E_R)\, dv\,, \tag{5}$$

where E_T is the threshold energy, the smallest recoil energy which the detector is capable of measuring, and $E_{\max}$ is the maximal recoil energy expressed in Eq. (2). Note that Eq. (5) holds only for an ideal detector in which the detector efficiencies, finite energy resolution effects, etc. are neglected.

The differential scattering cross section $\frac{d\sigma}{dE_R}(v, E_R)$ includes different types of WIMP-nucleus interactions. These interactions mainly depend on the WIMP-quark interaction strength, however, the resulting cross section is translated into the WIMP-nucleon cross section by using hadronic matrix elements which describe the nucleon content in terms of quarks and gluons. As intimated, two types of interaction are considered [26]: the spin-spin interaction (SD), where the WIMP couples to the spin of the nucleus by the exchange of a Z boson, and the scalar interaction (SI), where the WIMP couples to the mass of the nucleus by the exchange of a Higgs boson. In this work, we analyse the combination of both interactions:

$$\frac{d\sigma}{dE_R} = \left(\frac{d\sigma}{dE_R}\right)_{\rm SI} + \left(\frac{d\sigma}{dE_R}\right)_{\rm SD}\,. \tag{6}$$

The contributions of the SI WIMP-nucleus scattering result from the scalar and vector interaction terms in the Lagrangian. The presence of these, terms shown in Eq. (7), which include the couplings between SM particles and WIMP candidate, directly depends upon the particle physics model (see Ref. [29] for Feynman diagrams),

$$\mathcal{L}_{\rm SI} = \alpha_q^S \bar{\chi}\chi\bar{q}q + \alpha_q^V \bar{\chi}\gamma_\mu\chi\bar{q}\gamma^\mu q\,. \tag{7}$$

The SI differential cross section can be written as:

$$\left(\frac{d\sigma}{dE_R}\right)_{\rm SI} = \frac{m_N \sigma_0^{\rm SI} F^2(E_R)}{2\mu_N^2 v^2}\,, \tag{8}$$

where $F^2(E_R)$ is the nuclear form factor for SI interactions which is a Fourier transform of the nucleon density and parametrised in terms of the momentum transfer as [30]:

$$F^2(q) = \left(\frac{3j_1(qR_1)}{qR_1}\right)^2 \exp\left[-q^2 s^2\right], \tag{9}$$

where j_1 is a spherical Bessel function, $s \simeq 1$ fm is a measure of the nuclear skin thickness and $R_1 = \sqrt{R^2 - 5s^2}$ with $R \simeq 1.2\,A^{1/2}$ fm, A being the mass number of the nucleon. The form factor is normalised to unity at zero momentum transfer, $F(0) = 1$. Here, $\sigma_0^{\rm SI}$ is the SI zero momentum WIMP-nucleus cross section and leads to the following expression:

$$\sigma_0^{\rm SI} = \frac{4\mu_N^2}{\pi}\left[Zf^p + (A-Z)f^n\right]^2, \tag{10}$$

where Z is the nucleus atomic number, f_p and f_p are the WIMP-proton and WIMP-neutron couplings, respectively. In most cases the WIMP coupling to neutrons and protons is very similar, $f^p \approx f^n$, and Eq. (10) can be expressed as

$$\sigma_0^{\rm SI} = \frac{4\mu_N^2 A^2 f^p}{\pi}\,. \tag{11}$$

The SD scattering is due to the interaction of a WIMP with the spin of the nucleus through the part of the Lagrangian given by the axial-vector interaction terms such as

$$\mathcal{L}_{\rm SD} = \alpha_q^A (\bar{\chi}\gamma^\mu\gamma_5\chi)(\bar{q}\gamma_\mu\gamma_5 q)\,. \tag{12}$$

The SD differential cross section is [31]

$$\left(\frac{d\sigma}{dE_R}\right)_{\rm SD} = \frac{16 m_N}{\pi v^2}\Lambda^2 G_F^2 J(J+1)\frac{S(E_R)}{S(0)}\,, \tag{13}$$

where $F_{\rm SD}^2(E_R) = \frac{S(E_R)}{S(0)}$ is the SD form factor, which depends on the spin structure of a nucleus. Furthermore, $\Lambda = (a^n \langle S_n\rangle + a^p \langle S_p\rangle)/J$, where J is the spin of the target nucleus, $a^p(a^n)$ is the axial WIMP-proton(-neutron) coupling and $\langle S_p\rangle(\langle S_n\rangle)$ is the expectation value of the spin of protons (neutrons) in the nucleus. The SD form factors arise from nuclear models which describe the distribution of spins within the nucleus in response to the interaction and this can differ substantially depending upon a given target nucleus. In this work, we use the SD form factors given in Ref. [32]. The SD zero momentum cross section $\sigma_0^{\rm SD}$ can be expressed as:

$$\sigma_0^{\rm SD} = \frac{32}{\pi}\mu_N^2 \Lambda^2 G_F^2 J(J+1)\,. \tag{14}$$

As seen from Eqs. (11) and (14), the SI contribution is directly proportional to the square of the number of nucleons, A^2, whereas the SD one is a function of the nuclear angular momentum, $(J+1)/J$.

Finally, the total WIMP-nucleus cross section can be calculated by adding the gauge and scalar components shown in Eqs. (8) and (13). The form factor, $F(E_R)$, encodes the dependence on the momentum transfer, $q = \sqrt{2m_N E_R}$, and accounts for the coherence loss which leads to a suppression in the event rate for heavy WIMPs or nucleons. We can rewrite the differential cross section in Eq. (6) as

Table 1
The model-dependent DM benchmarks selected from the results shown in Figure 7 of Ref. [25] and used to generate direct detection signals.

DM benchmark	$m_{\chi_1^0}$ [GeV]	$\sigma_n^{\rm SI}$ [pb]	$\sigma_n^{\rm SD}$ [pb]	Composition [%]
BM-DPT I	1134	$1.07\text{x}10^{-11}$	$1.06\text{x}10^{-6}$	Higgsino-like, 98%
BM-DPT II	1181	$1.02\text{x}10^{-11}$	$1.67\text{x}10^{-6}$	Singlino-like, 96%
BM-DPT III	1161	$7.92\text{x}10^{-12}$	$1.83\text{x}10^{-6}$	Singlino-like, 96%
BM-DPT IV	1013	$7.83\text{x}10^{-12}$	$2.21\text{x}10^{-6}$	Singlino-like, 97%
BM-DPT V	1135	$2.01\text{x}10^{-11}$	$1.49\text{x}10^{-6}$	Singlino-like, 95%
BM-DPT VI	1114	$3.41\text{x}10^{-11}$	$1.54\text{x}10^{-6}$	Singlino-like, 95%

$$\frac{d\sigma}{dE_R} = \frac{m_N}{2\mu_N^2 v^2}\left(\sigma_0^{\rm SI} F_{\rm SI}^2(E_R) + \sigma_0^{\rm SD} F_{\rm SD}^2(E_R)\right). \tag{15}$$

In this work, we employ MicrOMEGAs (version 5.0.8) [33] to calculate the nuclear recoil spectrum shown in Eqs. (4) and (5). For the discrimination between the signal and background, it is needed to calculate the variance χ^2 [34,35]:

$$\chi^2 = \sum_{i=1}^{n}\left(\frac{N_i^{\rm tot} - N_i^{\rm bkg}}{\sigma_i}\right)^2, \tag{16}$$

where $N^{\rm tot} = N^{\rm sign} + N^{\rm bkg}$ is the total rate (per kilogram per day) measured by the detector, with $N^{\rm sign}$ and $N^{\rm bkg}$ the signal and background yields, respectively. However, we can also use this same χ^2 analysis to separate different type of signals in the case that we assume, e.g., one type of them being the nuclear recoil distribution for Higgsino-like neutralino (as signal) and the other one being the nuclear recoil distribution for Singlino-like neutralino (as background).

Of course, this presumes a signal being detected. With this in mind, we will divide the energy range between 5 and 50 keV in $n = 9$ equidistant energy bins. Here, we assume a Gaussian error $\sigma_i = \sqrt{\frac{N_i^{tot}}{M \cdot T}}$ on the measurement, where M is the detector mass and T the exposure time. We require $\chi^2 > 15.51$ to separate two direct detection signals at the 95% Confidence Level (CL). In our work we calculate χ^2 values and probe the discrimination of the direct detection signals, which results from different type of DM candidates, for four different exposures, $2\ t \cdot y$, $6\ t \cdot y$, $20\ t \cdot y$ and $200\ t \cdot y$. Especially, the exposures of $20\ t \cdot y$ and $200\ t \cdot y$ are the maximum expected exposures for the next generation direct detection experiments, XENONnT/LUX-ZEPLIN [36, 37] and DARWIN [38], respectively.

3. Results

In this section, we will present the results of our analysis on the comparison of DM direct detection signals, in presence of various nuclei, for different kinds of DM candidates in model-dependent and model-independent frameworks. In order to do so, we have selected some benchmarks in both frameworks, shown in Tables 1 and 2, respectively. The model-dependent benchmarks are selected from the UMSSM model results worked out in Ref. [25] while the model-independent ones, which do not result from any physical model, are created to compare the direct detection signals by varying arbitrarily the values of the SI and SD cross sections. For the Singlino-like benchmarks, the main annihilation channel of DM to get correct relic density is

Table 2
The model-independent DM benchmarks used to generate direct detection signals.

DM benchmark	m_χ [GeV]	$\sigma_n^{\rm SI}$ [pb]	$\sigma_n^{\rm SD}$ [pb]
BM-IND I	1000	$1.0\text{x}10^{-11}$	$1.0\text{x}10^{-6}$
BM-IND II	1000	$1.0\text{x}10^{-11}$	$1.5\text{x}10^{-6}$
BM-IND III	1000	$1.0\text{x}10^{-11}$	$2.0\text{x}10^{-6}$
BM-IND IV	1000	$1.0\text{x}10^{-11}$	$2.5\text{x}10^{-6}$
BM-IND V	1000	$1.5\text{x}10^{-11}$	$1.0\text{x}10^{-6}$
BM-IND VI	1000	$2.0\text{x}10^{-11}$	$1.0\text{x}10^{-6}$
BM-IND VII	1000	$2.5\text{x}10^{-11}$	$1.0\text{x}10^{-6}$

the production of the lightest Higgs state and Z boson via (off-shell) Z boson mediation. Also, the Bino and Wino masses, to which the DM nucleon interaction is sensitive, are larger than 10 TeV for all benchmarks in Table 1. In fact, the model dependent SI and SD cross sections shown in Table 1 are related to interaction terms in the model. The SD interaction terms for Higgsino- and Singlino-like DM depend on $(|N_{14}|^2 - |N_{15}|^2)$ and $|N_{16}|^2$, respectively. Here, $|N_{14}|^2$ and $|N_{15}|^2$ are the $\tilde{H}_u$ and $\tilde{H}_d$ components of the lightest neutralino while $|N_{16}|^2$ give the Singlino component. So, if one has a parameter space which satisfies all experimental bounds with $|N_{14}|^2 \sim |N_{15}|^2$, the SD cross sections for Singlino-like solutions would mostly be greater than the SD cross sections for Higgsino-like ones. The relevant relation can be seen in Figure 7 of [25]. Furthermore, neglecting the gaugino components, the SI interaction term which arise from SM-like Higgs mediated scattering shown in Eq. (7) depends on $N_{16}(N_{14} + N_{15})$, the mixing between Singlino and Higgsino. Unlike the SD case, we are not able to make an exact inference about the relation between the SI cross sections of Singlino- and Higgsino-like solutions. It can also be noted that we tried to choose model-independent benchmarks which have cross section and WIMP mass values similar to those of the model-dependent ones.

As seen from Table 1, there is only one Higgsino-like DM benchmark **BM-DPT I** with $|N_{14}|^2 \sim |N_{15}|^2$, whereas there are five Singlino-like DM benchmarks with various SI and SD cross sections. We will assess whether the described χ^2 analysis can *statistically* enable us to separate the former from the latter. Therefore, **BM-DPT I** can be regarded as our signal (in the sense discussed above) while the others are backgrounds. They all correspond to actual *discrete* parameter space points in the UMSSM. Conversely, the model-independent benchmarks shown in Table 2 are used to describe the typical *continuous* behaviour over the relevant recoil spectra.

In this analysis, the direct detection signals of the benchmarks shown in Tables 1 and 2 are calculated as the differential event rate in /keV/kg/day for a Xenon, Germanium and Silicon target nucleus. Each detector composed of these targets surely has different experimental backgrounds. The experimentalists deal with reducing these backgrounds in direct detection experiments to increase sensitivity. In this work, however, we assume that our signals are larger than the experimental backgrounds and any uncertainties are suppressed since we intend to focus on the discrimination between the expected direct detection signals of two different DM candidates, one Higgsino- and the other Singlino-like. In the forthcoming figures, for each type of target, the model-independent differential event distributions are displayed in large plots in the top panels. In these plots, a black line refers to the distribution for the benchmark **BM-IND I** while the rates for other benchmarks are tagged as coloured lines. The small plots in the top panels indicate instead the ratio of the coloured lines to the black signal with the same colour coding.

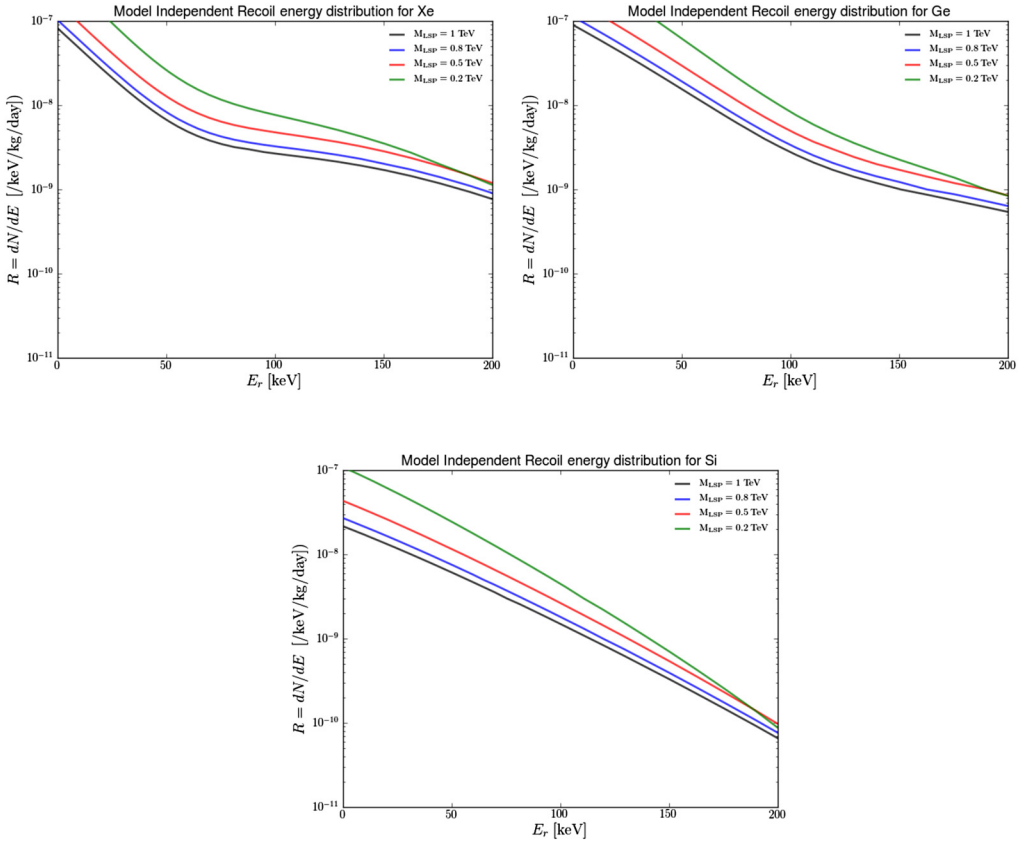

Fig. 1. The direct detection signals of the benchmarks with varying neutralino LSP masses and same SI and SD cross sections ($\sigma_n^{\rm SI} = 10^{-11}$ and $\sigma_n^{\rm SD} = 10^{-6}$) as a function of the nucleus recoil energy ($E_r \equiv E_R$) for Xenon (top left panel), Germanium (top right panel) and Silicon (bottom panel) targets. We use the standard Maxwellian isothermal model with $\rho_0 = 0.3$ GeV/cm^3. The colour coding can be read from the legend of the plots. (For interpretation of the colours in the figure(s), the reader is referred to the web version of this article.)

In the model-dependent case shown in the bottom panels, the colour coding is same as with the model-independent case and we show only the plots with the ratio of coloured rates to black signal (again, corresponding to the benchmark **BM-DPT I**). In both cases, the right (left) panels display the different recoil shapes of signals according to varying SI (SD) cross sections.

Before presenting the results of our detailed analysis on the direct detection of the LSP neutralinos with different compositions, in Fig. 1, we show the direct detection signals of the model-independent benchmarks with varying neutralino LSP masses and same SI and SD cross sections ($\sigma_n^{\rm SI} = 10^{-11}$ and $\sigma_n^{\rm SD} = 10^{-6}$) as a function of the nucleus recoil energy ($E_r \equiv E_R$) for Xenon (top left panel), Germanium (top right panel) and Silicon (bottom panel) targets. As expected from Eq. (4), the lighter the DM the larger the differential event rate. Furthermore, according to the figure, the shape of the recoil energy distributions varies with the type of target material.

Fig. 2 shows the direct detection signals of the benchmarks shown in Tables 1 and 2 for a Xenon target nucleus with the mass number of 131. According to the top left panels, the effect of

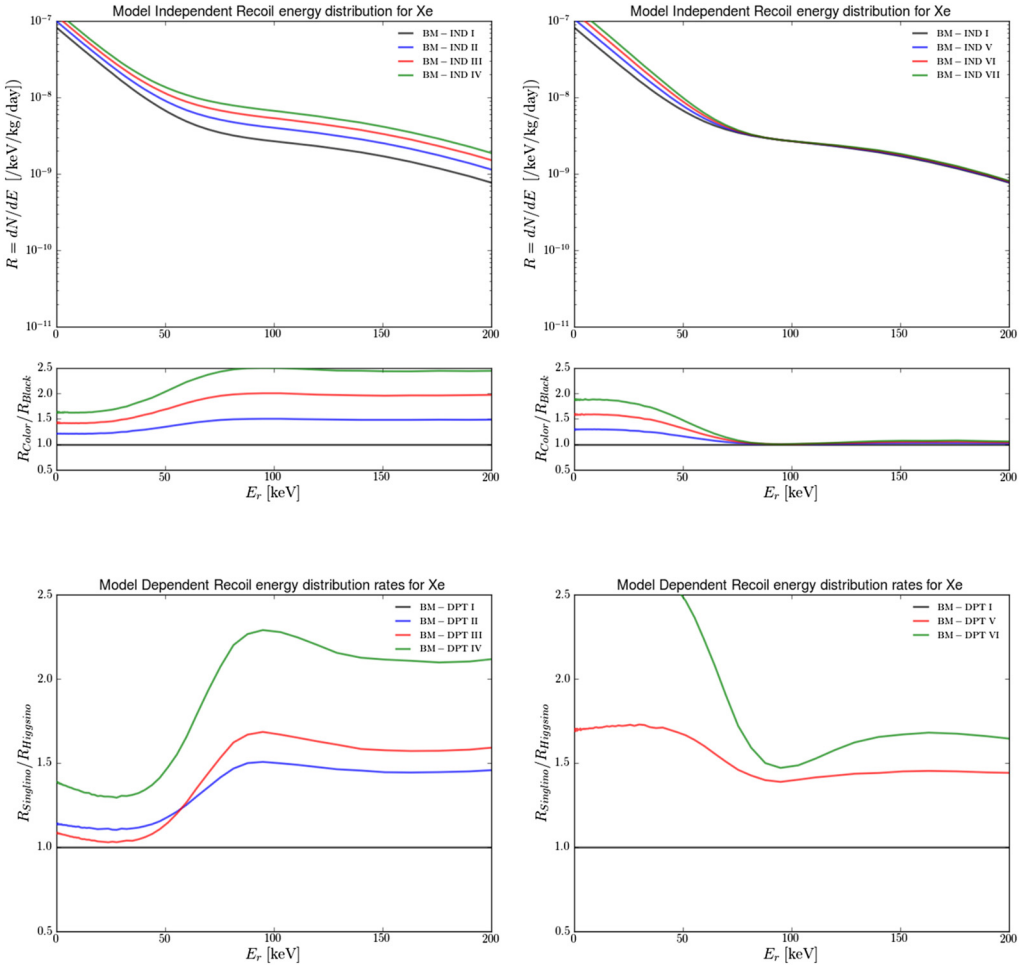

Fig. 2. The direct detection signals of the benchmarks shown in Tables 1 and 2 as a function of the nucleus recoil energy ($E_r \equiv E_R$) for a Xenon target. We use the standard Maxwellian isothermal model with $\rho_0 = 0.3$ GeV/cm^3. The model-independent differential event distributions are displayed in the large plots of the top panels. In these plots, a black line refers to the benchmark **BM-IND I** while the other benchmarks are tagged in coloured lines. The small plots of the top panels indicate the ratio of the coloured benchmarks to the black one. In the model-dependent case shown in the bottom panels, the colour coding is the same as in the model-independent case but we only show the plots with the ratios of the benchmarks. For both cases, the right (left) panels display the different recoil spectra according to varying SI (SD) cross sections.

changing the SD cross section on the difference between black and any coloured signal is small up to 50 keV of the nuclear recoil energy, compared to the rate of changing the SD cross section. For larger recoil energies, the coloured to black signal ratio, shown in the small plots in the top panels, approximates the ratio between the SD cross sections of two signals. The reason is due to the distribution of the SI nuclear form factor for the Xenon atom shown in Eq. (9). According to Ref. [27], the value of the SI nuclear form factor drops significantly for a Xenon target as the nuclear recoil energy increases. Therefore, the contribution of the SI interaction cross section to the event rate shown in Eq. (15) decreases rapidly for larger recoil energies, although Xenon has

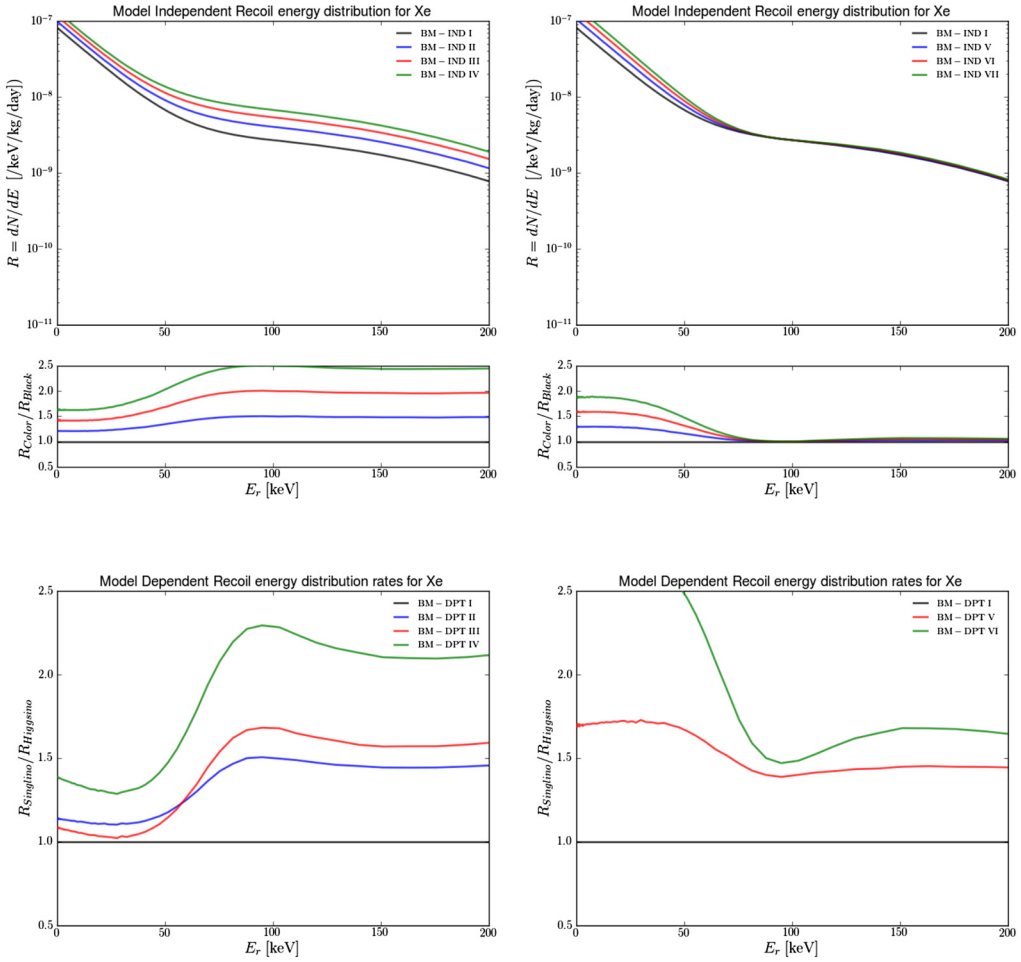

Fig. 3. Same as in Fig. 2 for the SHM++ distribution model with $\rho_0 = 0.55 \pm 0.17$ GeV/cm^3.

large a mass number of nucleon, A, upon which the SI zero-momentum cross section shown in Eq. (11) depends. In the case of varying SI cross sections with same DM masses and SD cross sections (top right panel), it can be noted that the aforementioned result is verified, since it seems that there is no difference between the signals with same SD cross sections for larger recoil energy. When we look at the ratio between the model-dependent distributions (bottom panels), it can easily be seen that the variation in the SI cross sections shown in Table 1 largely affects the difference of the direct detection signals for smaller recoil energies than about 50 keV, as the SD cross section becomes important for larger recoil energies.

The main energy range for the signal in the direct detection experiments with Xenon target has generally been between the recoil energies of 5 and 50 keV [36]. Looking at the results of Fig. 2, it can be concluded that the SI cross sections of the DM candidates play a more significant role than the SD cross sections in determining the type of DM in direct detection experiments with Xenon target. Moreover, in Figs. 3 and 4, we compose the recoil spectrum shown in Fig. 2 for different WIMP velocity distribution models and SD form factors. It can be noted that the

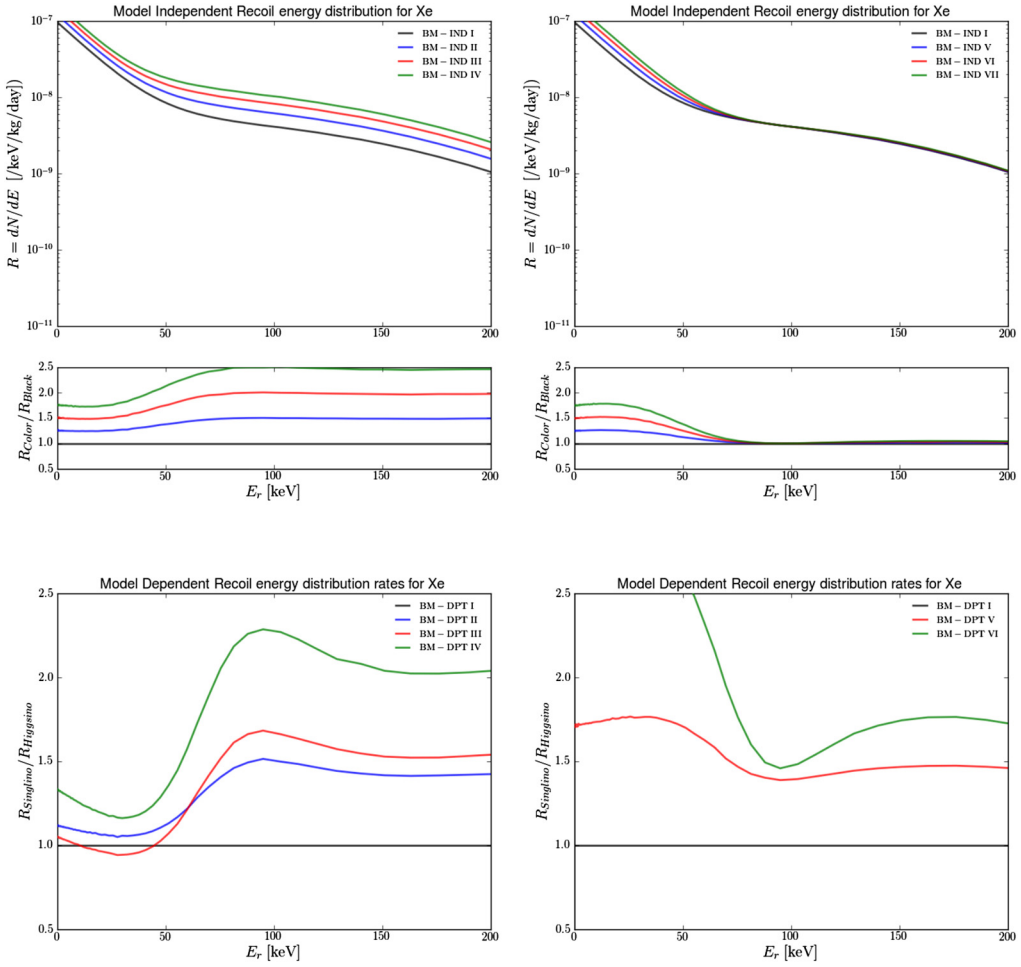

Fig. 4. Same as in Fig. 2 for a different SD form factor.

shape of the Xenon recoil spectrum and normalisation of the signals shown in the bottom panels are almost the same in all these figures. In Table 3, we display the χ^2 values of the benchmarks shown in Fig. 2 for the exposures of 20 $t \cdot y$ and 200 $t \cdot y$, the proposed maximum exposures for the upcoming direct detection experiments XENONnT/LUX-ZEPLIN [36,37] and DARWIN [38], respectively. According to the table, separating the black benchmark from the coloured ones with varying SI or SD cross sections and same masses cannot generally be possible for exposure of 20 $t \cdot y$ (i.e., in the near future) while exposure of 200 $t \cdot y$ (i.e., in the far future) can easily provide the separation conditions for the various DM assumptions. Certainly, though, the larger gaps between the signals which belong to different DM candidates can be exploited in presence of exposures of 20 $t \cdot y$, as documented in the last χ^2 result of the bottom right panel.

In Fig. 5, we extend the previous analysis to the case of a Germanium target nucleus with a mass number of 73. Unlike the case of a Xenon target nucleus (with a mass number of 131), the effect of the SI cross section on the differentiation of the signals is quite small for the whole range of nuclear recoil energies (top right panel), since the SI zero-momentum cross section shown in

Table 3
χ^2 values for the panels in Fig. 2.

N_{sign}/N_{bkg}	χ^2 values for top left panel		χ^2 values for top right panel	
	$\chi^2(20\,t\cdot y)$	$\chi^2(200\,t\cdot y)$	$\chi^2(20\,t\cdot y)$	$\chi^2(200\,t\cdot y)$
Blue/Black	0.97	9.75	1.74	17.49
Red/Black	3.32	33.25	5.71	57.13
Green/Black	6.51	65.18	10.86	108.62
N_{sign}/N_{bkg}	χ^2 values for bottom left panel		χ^2 values for bottom right panel	
	$\chi^2(20\,t\cdot y)$	$\chi^2(200\,t\cdot y)$	$\chi^2(20\,t\cdot y)$	$\chi^2(200\,t\cdot y)$
Blue/Black	0.39	3.93	–	–
Red/Black	0.15	1.53	6.65	66.55
Green/Black	2.51	25.11	22.53	225.39

Table 4
χ^2 values for the panels in Fig. 5.

N_{sign}/N_{bkg}	χ^2 values for top left panel		χ^2 values for top right panel	
	$\chi^2(20\,t\cdot y)$	$\chi^2(200\,t\cdot y)$	$\chi^2(20\,t\cdot y)$	$\chi^2(200\,t\cdot y)$
Blue/Black	3.59	35.98	0.18	1.85
Red/Black	11.12	111.20	0.68	6.87
Green/Black	20.38	203.84	1.44	14.44
N_{sign}/N_{bkg}	χ^2 values for bottom left panel		χ^2 values for bottom right panel	
	$\chi^2(20\,t\cdot y)$	$\chi^2(200\,t\cdot y)$	$\chi^2(20\,t\cdot y)$	$\chi^2(200\,t\cdot y)$
Blue/Black	2.12	21.27	–	–
Red/Black	3.13	31.36	3.45	34.53
Green/Black	10.27	102.76	8.23	82.31

Eq. (11) is proportional to the square of the atomic mass number (as already mentioned). Beside this, the scaling factor of Germanium for the SD cross sections, $(J+1)/J$, is larger than for Xenon [39]. This also ensures a event rate at the same level as with Xenon. In short, the difference between the SD cross sections of DM candidates gives a dominant contribution to be able to separate those signals from each other in the direct detection experiments with a Germanium target (top left and bottom left panels). Due to the same reason, unlike Fig. 6, the changes in the SD form factor give rise to visible differences in the recoil spectrum as seen in Fig. 7. The χ^2 values for the distributions in Fig. 5 are presented in Table 4 and the most interesting result is that the recoil signals of two DM candidates with same SD cross sections cannot be discriminated in direct detection experiments with a Germanium target even for an exposure of 200 $t\cdot y$ (these are the χ^2 values for the top right panel). Fig. 6.

Fig. 8, showing the nuclear recoil distributions for a Silicon target nucleus with mass number of 29, leads to conclusions similar to those of the Germanium case. However, as shown in Table 5, differentiating the recoil distributions of different DM candidates in a Silicon detector is harder, since the event rate is lower than for Germanium due to the smaller mass number and also scaling factor for the SD cross section. As seen from Fig. 9 and Fig. 10, the shape of the Silicon recoil spectrum and normalisation of the signals can not be separated for different DM velocity distribution and SD form factors. Moreover, in Tables 3–5, it is clear that the χ^2 values obtained for a given set of two benchmarks simply scale linearly with the exposure due to taking into account only the Gaussian error of the signal. In the case of negligible backgrounds and un-

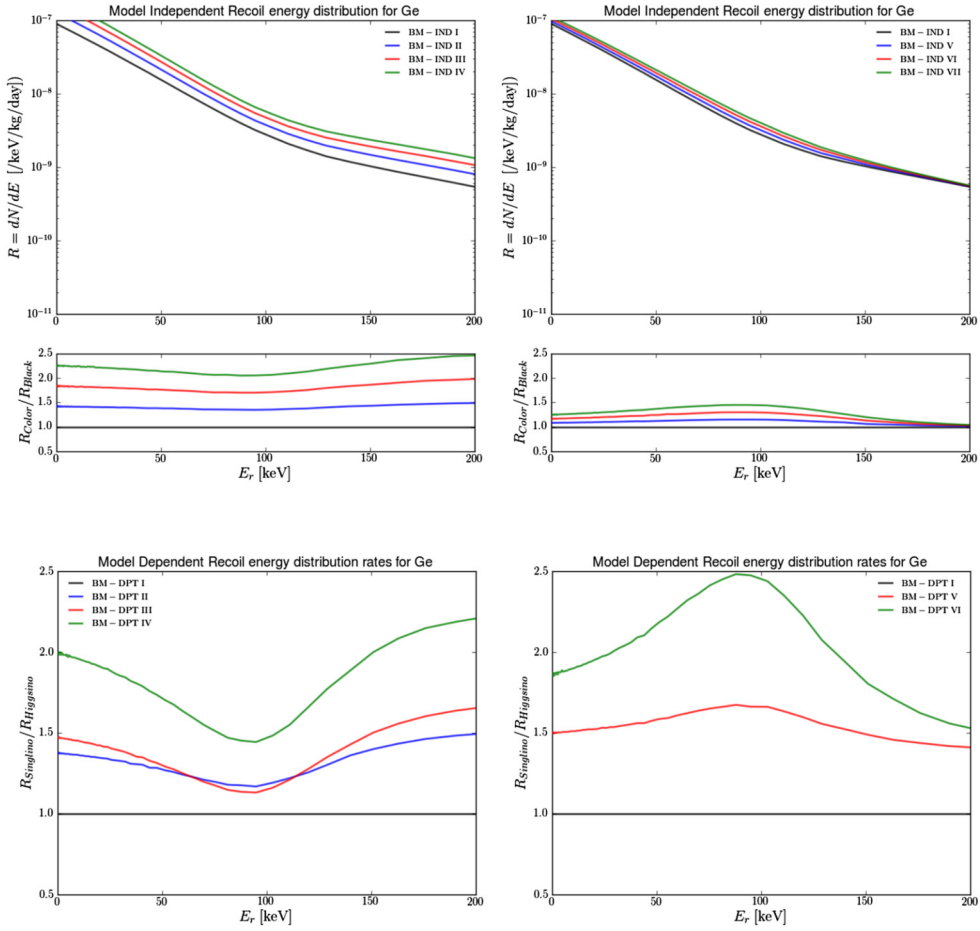

Fig. 5. Same as in Fig. 2 for Germanium.

Table 5
χ^2 values for the panels in Fig. 8.

N_{sign}/N_{bkg}	χ^2 values for top left panel		χ^2 values for top right panel	
	$\chi^2(20\,t\cdot y)$	$\chi^2(200\,t\cdot y)$	$\chi^2(20\,t\cdot y)$	$\chi^2(200\,t\cdot y)$
Blue/Black	0.97	9.72	0.019	0.19
Red/Black	2.97	29.72	0.074	0.74
Green/Black	5.41	54.12	0.16	1.60
N_{sign}/N_{bkg}	χ^2 values for bottom left panel		χ^2 values for bottom right panel	
	$\chi^2(20\,t\cdot y)$	$\chi^2(200\,t\cdot y)$	$\chi^2(20\,t\cdot y)$	$\chi^2(200\,t\cdot y)$
Blue/Black	0.95	9.56	–	–
Red/Black	1.50	15.09	0.95	9.58
Green/Black	4.41	44.18	1.80	18.08

certainties, this simple scaling could also be useful to calculate the exposure needed to separate different benchmarks.

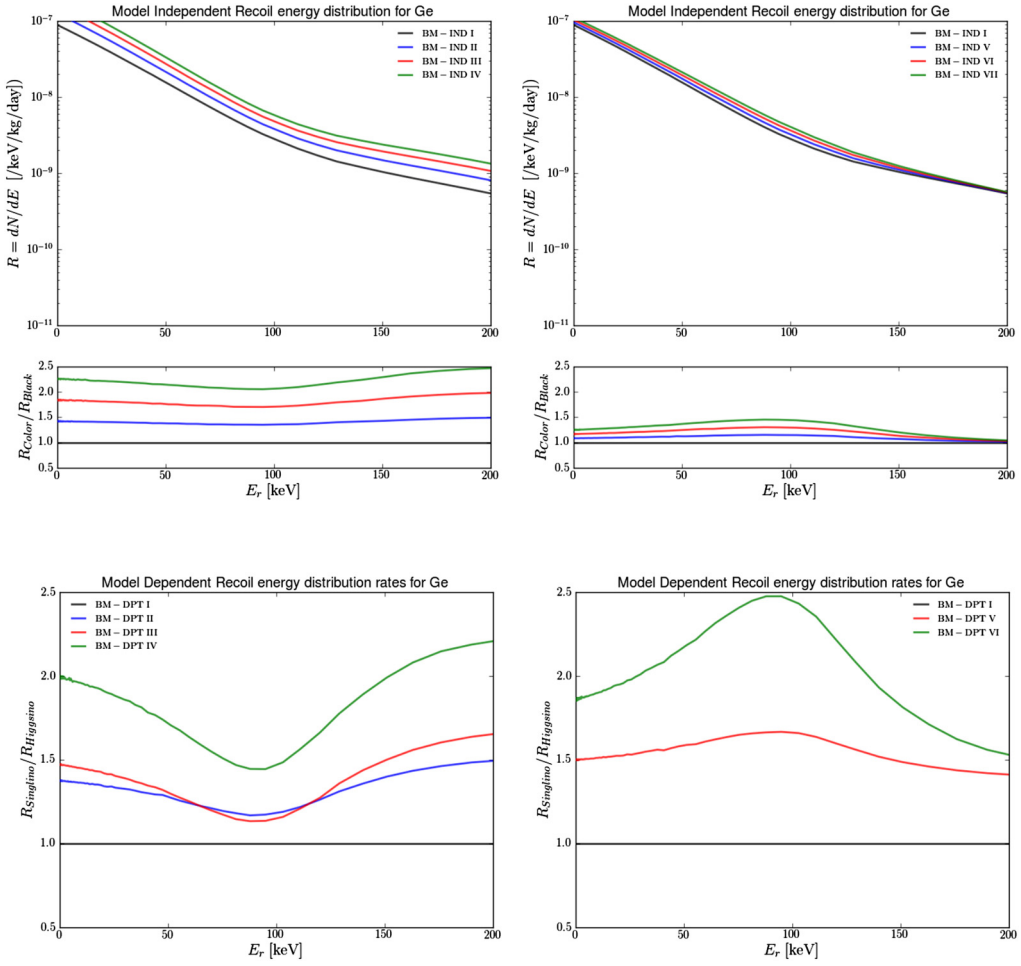

Fig. 6. Same as in Fig. 3 for Germanium.

In the remainder of our analysis, we investigate that how the ratio between the total number of nuclear recoil events of the Singlino- and Higgsino-like DM neutralinos changes in terms of different exposures. In this part, we only use the model-dependent results, which satisfy all experimental bounds, shown in Figure 7 of Ref. [25]. The plots in Fig. 11 show the ratio between Singlino- and Higgsino-like DM masses in the range of [0.99,1.01] versus the ratio between Singlino- and Higgsino-like DM total number of events between 5 and 50 keV nuclear recoil energy for Xenon (top left panel), Germanium (top right panel) and Silicon (bottom panel) targets. The yellow, purple, green and red points shows the regions over which the nuclear recoil distributions, which are derived from the parameter space of the UMSSM model, can be separable for $2\ t\cdot y$, $6\ t\cdot y$, $20\ t\cdot y$ and $200\ t\cdot y$ exposures, while the blue points refer to the case when this cannot be done via our χ^2 analysis. The following list summarises the relation between colours and exposures in Fig. 11.

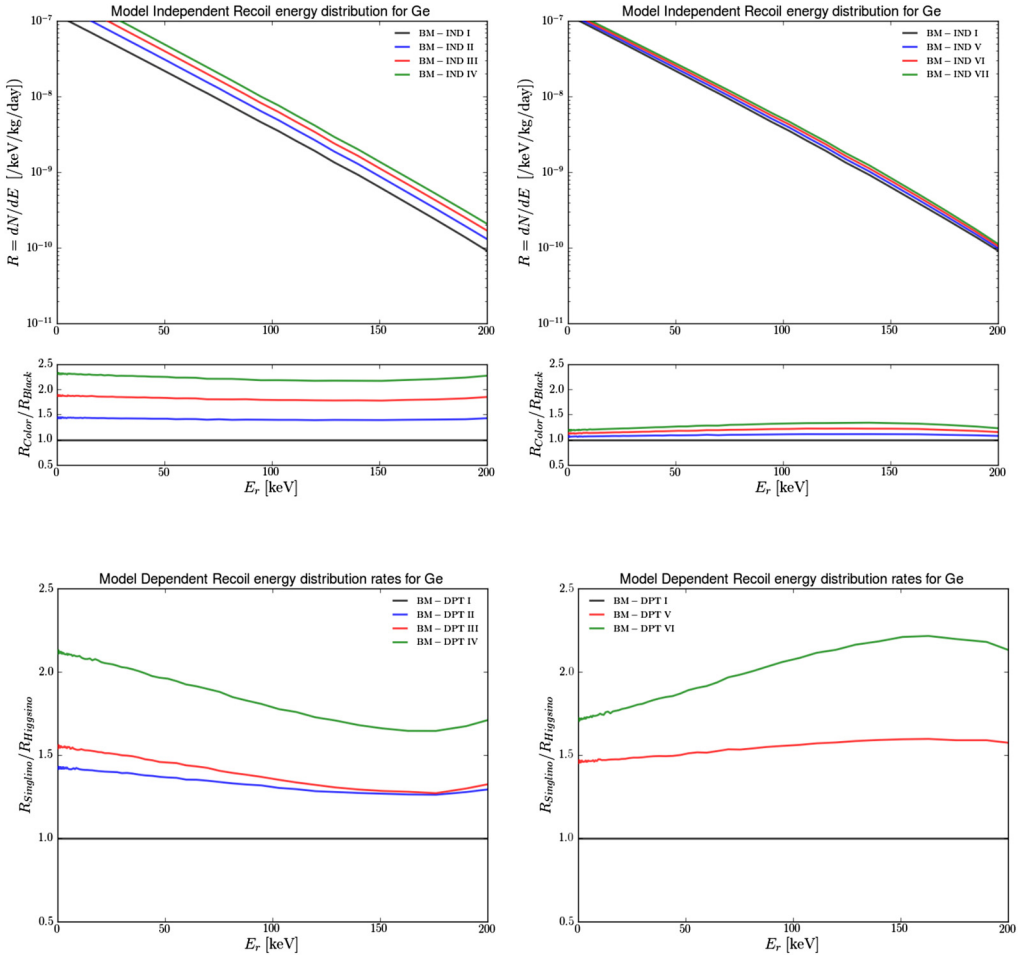

Fig. 7. Same as in Fig. 4 for Germanium.

- Yellow: The nuclear recoil spectra can be separable with an exposure of 2 $t \cdot y$.
- Yellow+Purple: The nuclear recoil spectra can be separable with an exposure of 6 $t \cdot y$.
- Yellow+Purple+Green: The nuclear recoil spectra can be separable with an exposure of 20 $t \cdot y$.
- Yellow+Purple+Green+Red: The nuclear recoil spectra can be separable with an exposure of 200 $t \cdot y$.
- Blue: The nuclear recoil spectra cannot be separable.

Clearly, when the total (SD plus SI) event rate is very similar for Singlino- and Higgsino-like DM, separation of these two DM candidates is not really possible, irrespectively of their mass

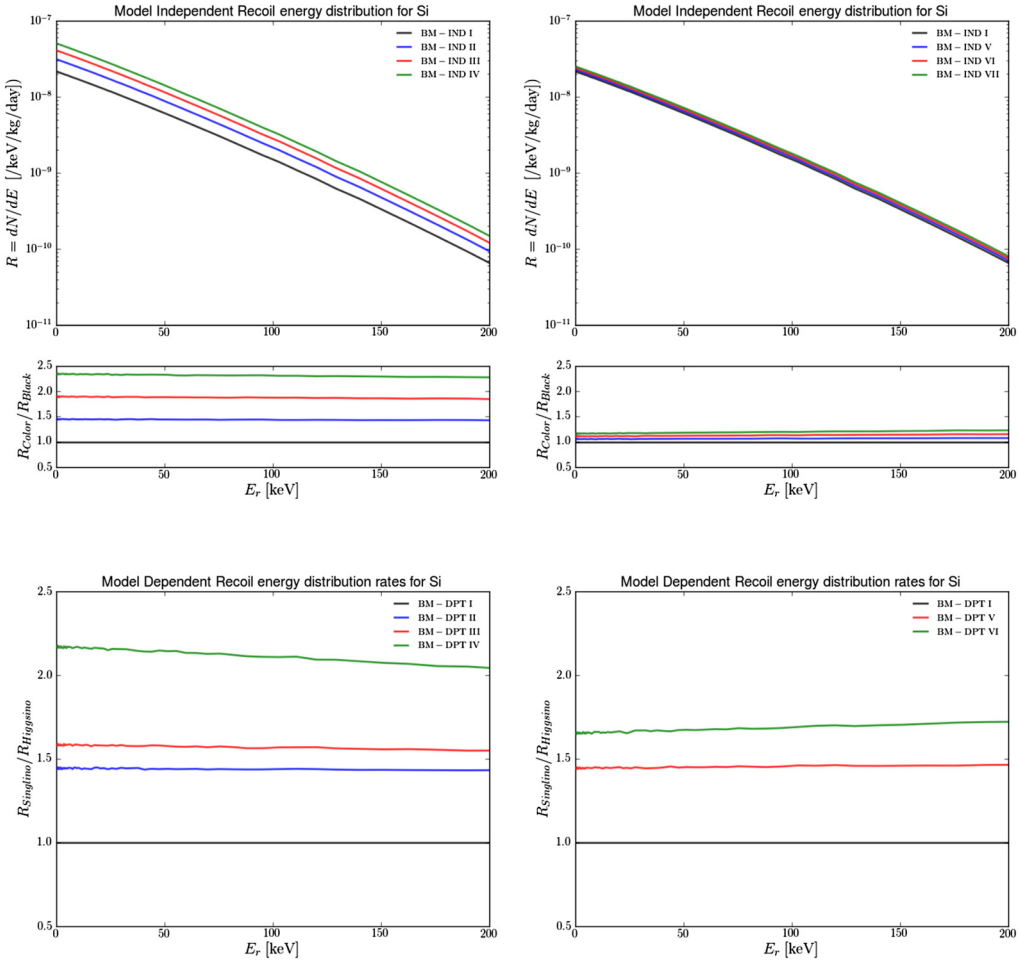

Fig. 8. Same as in Fig. 2 for Silicon.

ratio. Conversely, even when the latter is close to one, separation is indeed possible even for small event rate differences so long that sufficient exposure is afforded by the experiment. Here, a detector exploiting Xenon would overall be better placed than one using Germanium or Silicon, as less exposure is needed to achieve a similar level of separation of the DM nature.

4. Conclusions

In this work, we have shown that a χ^2 analysis usually adopted in separating DM signals from backgrounds in case of direct detection experiments, when a signal has indeed been established, can also be used to distinguish the nature of the DM candidate. Specifically, we have shown that Singlino- and Higgsino-like signals emerging from a UMSSM model of E_6 origin can be distinguished from each other. While we have shown this to be the case in this model-dependent example, we have also used a model-independent setup to provide a backdrop illustrating the origin of such a difference, using a variety of materials used in such DM experiments.

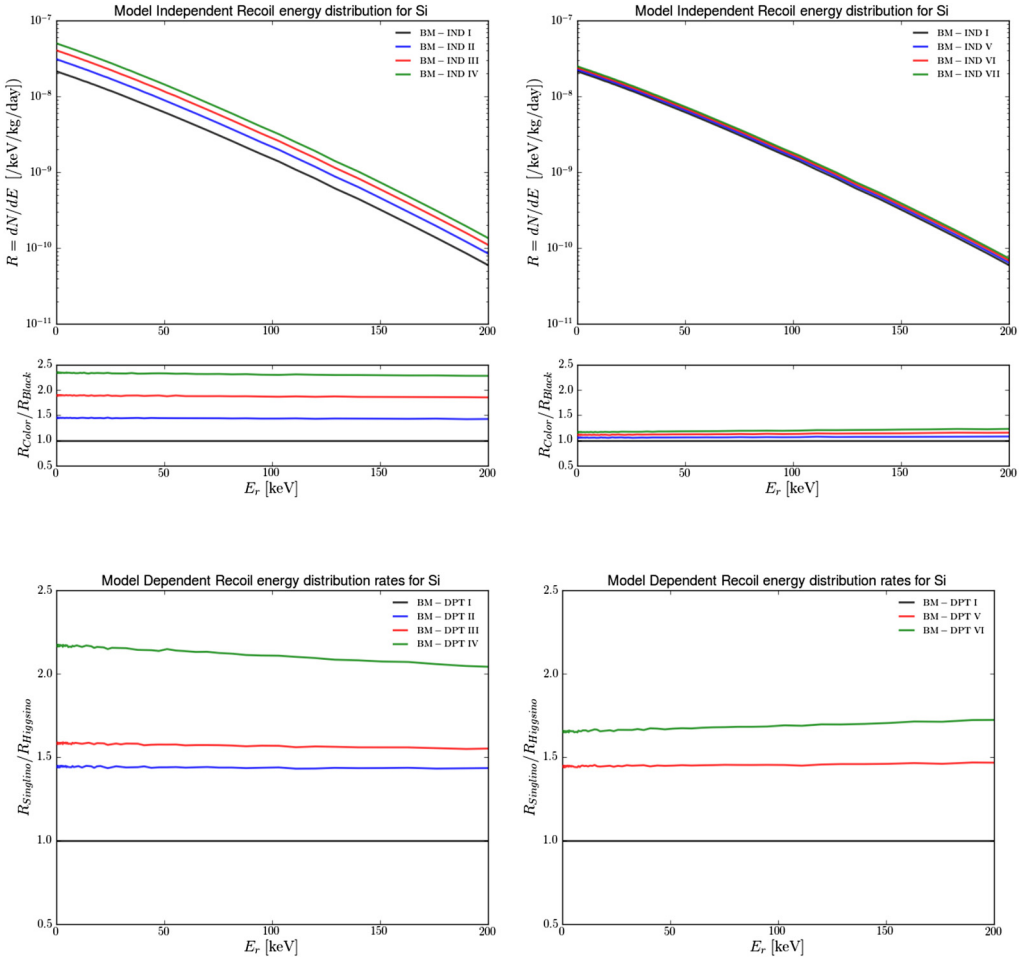

Fig. 9. Same as in Fig. 3 for Silicon.

Specifically, we have found that varying the SI cross sections largely impacts the difference between the signals in Xenon detectors while it is insufficient in the case of Germanium and Silicon ones. In the latter detectors, instead, varying SD cross sections have a powerful effect in order to discriminate the evidenced signals from the two DM candidates. On the one hand, this means that it cannot be possible to extract the DM nature in Xenon detectors in case of similar scalar and vector interactions. On the other hand, in Germanium and Silicon detectors, the same is true for the DM candidates with similar axial-vector interactions. Hence, different detector materials are differently suited in direct detection experiments in extracting the nature of a detected DM signal.

CRediT authorship contribution statement

Yaşar Hiçyılmaz: Data curation, Software, Visualization, Writing – original draft. **Stefano Moretti:** Conceptualization, Project administration, Supervision, Writing – review & editing.

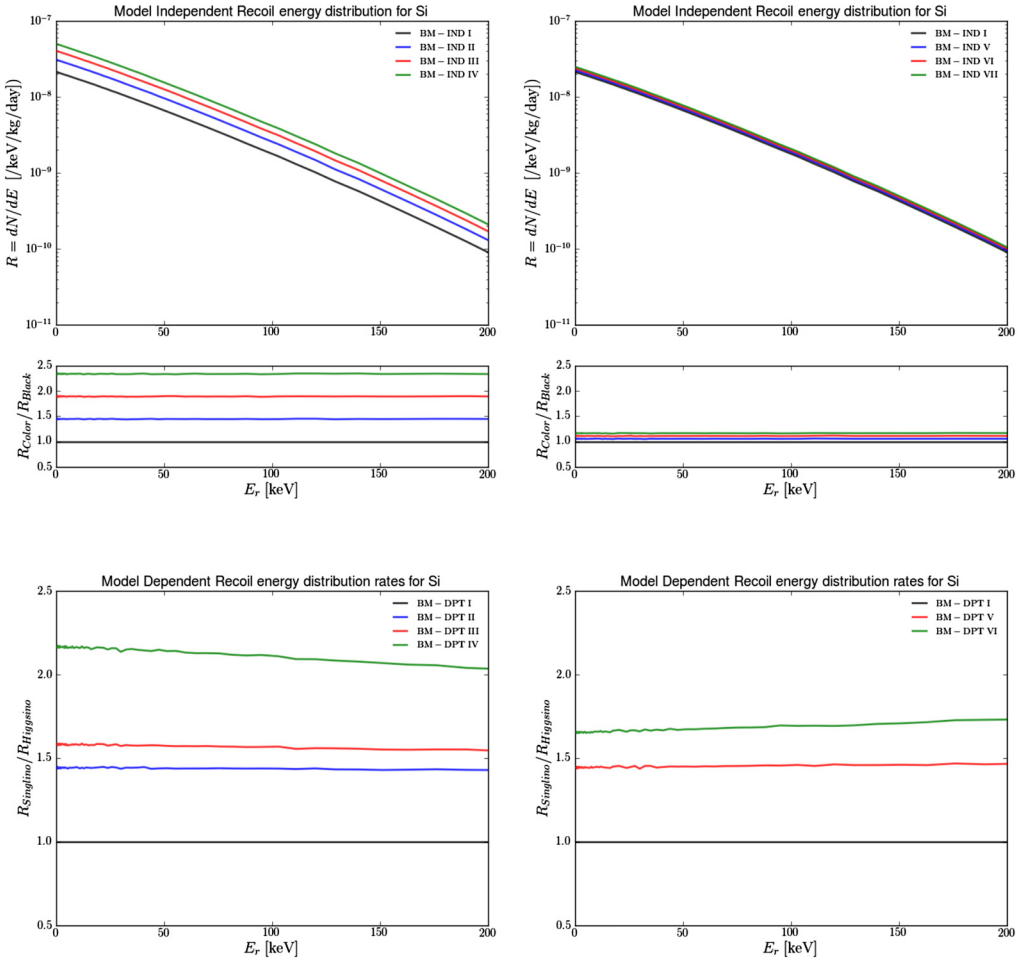

Fig. 10. Same as in Fig. 4 for Silicon.

Declaration of competing interest

The authors declare that they have no known competing financial interests or personal relationships that could have appeared to influence the work reported in this paper.

Acknowledgements

SM is supported in part through the NExT Institute and the STFC consolidated Grant No. ST/L000296/1. The work of YH is supported by the Scientific and Technological Research Council of Turkey (TUBITAK) in the framework of 2219-International Postdoctoral Research Fellowship Program. The authors also acknowledge the use of the IRIDIS High Performance Computing Facility, and associated support services at the University of Southampton, in the completion of this work.

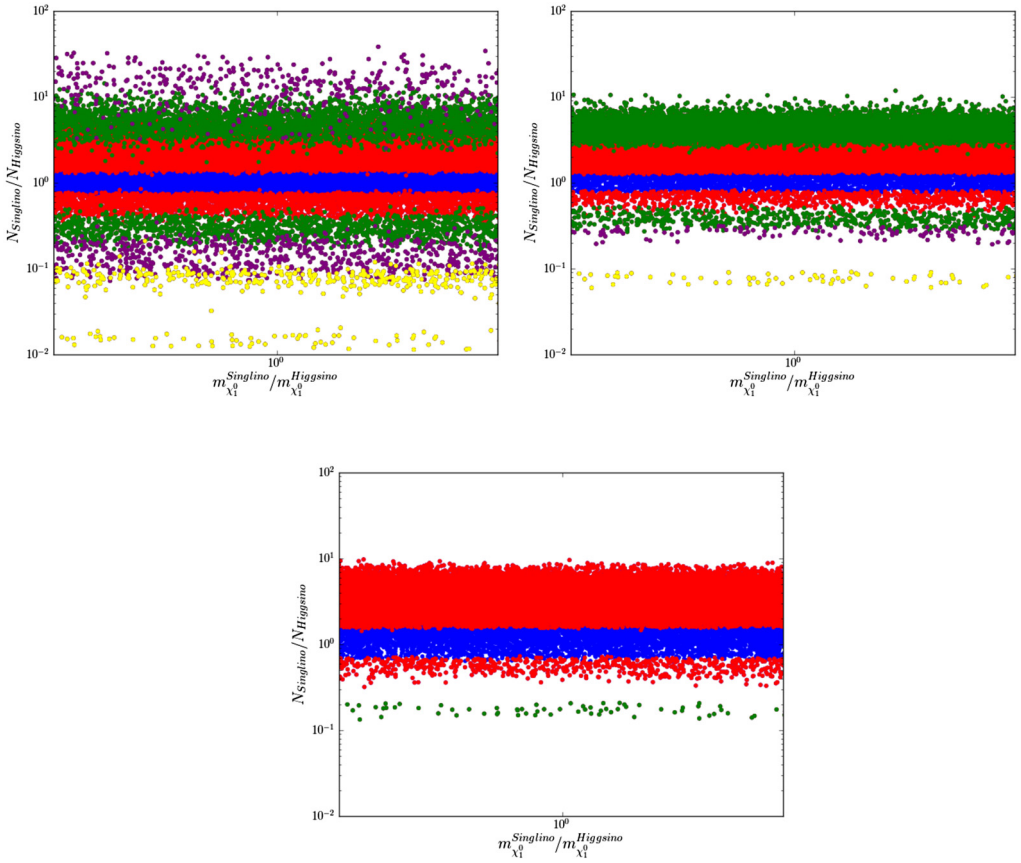

Fig. 11. The ratio between Singlino- and Higgsino-like DM masses in the range of [0.99,1.01] versus the ratio between Singlino- and Higgsino-like DM total number of events between 5 and 50 keV nuclear recoil energy for Xenon (top left panel), Germanium (top right panel) and Silicon (bottom panel) targets. The yellow, purple, green and red points show the regions that the nuclear recoil distributions, which are derived from the parameter space of the UMSSM model, can be separable for 2 $t \cdot y$, 6 $t \cdot y$, 20 $t \cdot y$ and 200 $t \cdot y$ exposures, respectively, while the blue points refer to that case when this is not possible with our χ^2 analysis. The colour coding is detailed in the text.

References

[1] F. Zwicky, Helv. Phys. Acta 6 (1933) 110.
[2] D.N. Schramm, Philos. Trans. R. Soc. Lond. A 307 (1982) 43.
[3] P.A.R. Ade, et al., Planck, Astron. Astrophys. 594 (2016) A13, arXiv:1502.01589 [astro-ph.CO].
[4] C.L. Bennett, et al., WMAP, Astrophys. J. Suppl. Ser. 208 (2013) 20, arXiv:1212.5225 [astro-ph.CO].
[5] D. Alvisi, et al., Nucl. Instrum. Methods Phys. Res., Sect. A 437 (1999) 212.
[6] M. Ackermann, et al., Fermi-LAT, Phys. Rev. Lett. 115 (2015) 231301, arXiv:1503.02641 [astro-ph.HE].
[7] G. Sullivan, IceCube, Nucl. Phys. B, Proc. Suppl. 235–236 (2013) 346, arXiv:1210.4195 [astro-ph.HE].
[8] E. Aprile, et al., XENON, Phys. Rev. Lett. 121 (2018) 111302, arXiv:1805.12562 [astro-ph.CO].
[9] X. Cui, et al., PandaX-II, Phys. Rev. Lett. 119 (2017) 181302, arXiv:1708.06917 [astro-ph.CO].
[10] H.S. Lee, et al., Phys. Rev. D 90 (2014) 052006, arXiv:1404.3443 [astro-ph.CO].
[11] R. Agnese, et al., SuperCDMS, Phys. Rev. D 97 (2018) 022002, arXiv:1707.01632 [astro-ph.CO].
[12] R. Agnese, et al., SuperCDMS, Phys. Rev. Lett. 120 (2018) 061802, arXiv:1708.08869 [hep-ex].
[13] E. Behnke, et al., COUPP, Phys. Rev. D 86 (2012) 052001, arXiv:1204.3094 [astro-ph.CO].
[14] E. Behnke, et al., PICASSO, Astropart. Phys. 90 (2017) 85, arXiv:1611.01499 [hep-ex].

[15] C. Amole, et al., PICO, Phys. Rev. D 93 (2016) 052014, arXiv:1510.07754 [hep-ex].
[16] C. Amole, et al., PICO, Phys. Rev. Lett. 118 (2017) 251301, arXiv:1702.07666 [astro-ph.CO].
[17] G. Angloher, et al., CRESST, Eur. Phys. J. C 76 (2016) 25, arXiv:1509.01515 [astro-ph.CO].
[18] L.T. Yang, et al., CDEX, Chin. Phys. C 42 (2018) 023002, arXiv:1710.06650 [hep-ex].
[19] A. Aguilar-Arevalo, et al., DAMIC, Phys. Rev. D 94 (2016) 082006, arXiv:1607.07410 [astro-ph.CO].
[20] D.S. Akerib, et al., LUX, Phys. Rev. Lett. 112 (2014) 091303, arXiv:1310.8214 [astro-ph.CO].
[21] A.H.G. Peter, V. Gluscevic, A.M. Green, B.J. Kavanagh, S.K. Lee, Phys. Dark Universe 5–6 (2014) 45–74, arXiv:1310.7039 [astro-ph.CO].
[22] V. Gluscevic, M.I. Gresham, S.D. McDermott, A.H.G. Peter, K.M. Zurek, J. Cosmol. Astropart. Phys. 12 (2015) 057, arXiv:1506.04454 [hep-ph].
[23] F. Kahlhoefer, S. Wild, J. Cosmol. Astropart. Phys. 10 (2016) 032, arXiv:1607.04418 [hep-ph].
[24] T.D.P. Edwards, B.J. Kavanagh, C. Weniger, Phys. Rev. Lett. 121 (18) (2018) 181101, arXiv:1805.04117 [hep-ph].
[25] M. Frank, Y. Hicyılmaz, S. Moretti, Ö. Özdal, J. High Energy Phys. 05 (2020) 123, arXiv:2004.01415 [hep-ph].
[26] M.W. Goodman, E. Witten, Phys. Rev. D 31 (1985) 3059.
[27] J.D. Lewin, P.F. Smith, Astropart. Phys. 6 (1996) 87.
[28] N.W. Evans, C.A.J. O'Hare, C. McCabe, Phys. Rev. D 99 (2) (2019) 023012, https://doi.org/10.1103/PhysRevD.99.023012, arXiv:1810.11468 [astro-ph.GA].
[29] G. Jungman, M. Kamionkowski, K. Griest, Phys. Rep. 267 (1996) 195, arXiv:hep-ph/9506380 [hep-ph].
[30] J. Engel, Phys. Lett. B 264 (1991) 114.
[31] M. Pato, J. Cosmol. Astropart. Phys. 10 (2011) 035, arXiv:1106.0743 [astro-ph.CO].
[32] G. Belanger, F. Boudjema, A. Pukhov, A. Semenov, Comput. Phys. Commun. 180 (2009) 747–767, arXiv:0803.2360 [hep-ph].
[33] G. Bélanger, F. Boudjema, A. Goudelis, A. Pukhov, B. Zaldivar, Comput. Phys. Commun. 231 (2018) 173, arXiv:1801.03509 [hep-ph].
[34] N. Bernal, J. Cosmol. Astropart. Phys. 08 (2009) 022, arXiv:0905.4239 [hep-ph].
[35] S. Profumo, K. Sigurdson, L. Ubaldi, J. Cosmol. Astropart. Phys. 12 (2009) 016, arXiv:0907.4374 [hep-ph].
[36] E. Aprile, et al., XENON, J. Cosmol. Astropart. Phys. 04 (2016) 027, arXiv:1512.07501 [physics.ins-det].
[37] B.J. Mount, et al., LUX-ZEPLIN, arXiv:1703.09144 [physics.ins-det].
[38] J. Aalbers, et al., DARWIN, J. Cosmol. Astropart. Phys. 11 (2016) 017, arXiv:1606.07001 [astro-ph.IM].
[39] R.W. Schnee, arXiv:1101.5205 [astro-ph.CO].